

(BBL),¹⁴ and cLPs derived from perylene-3,4,9,10-tetracarboxylic acid diimides (PDIs),¹⁵ carbazole¹⁶ or fluorene¹⁷ moieties, as well as those ladder structures bridged by intramolecular coordinate bonds.^{18,19} cLPs are promising materials for a wide range of applications, such as photodetectors,²⁰ light emitting diodes,²¹ field-effect transistors,²² thermoelectric devices,²³ and high performance organic photovoltaics.^{24–28} For most of these applications, cLPs demonstrated significantly higher stability compared to their non-ladder counterparts thanks to the presence of multiple strands of bonds and the thermodynamically stable fused-ring aromatic backbones.

The chain rigidity of conjugated polymers greatly influences their physical properties and hence electronic performance. With an extra strand of bonds, cLPs are expected to have a stiffer backbone because the additional strand of bonds along the backbone hinders the torsional motion in the mainchain.²⁹ Such an enhanced rigidity often leads to lower backbone conformational entropy³⁰ and stronger interchain interactions. Consequently, cLPs generally exhibit lower solubility compared with non-ladder conjugated polymers due to their lower entropy gain³¹ and higher required enthalpy change needed to break the strong inter-chain interactions during the dissolving process. In this context, the solution properties of cLPs, such as chain conformation and solution aggregation, are less explored compared with those of non-ladder-shaped conjugated polymers.

In the present work, we thoroughly examined the solution properties of a carbazole-derived cLP (**LP**), by comparing with a control polymer **CP** without a ladder component, by variable-temperature UV-vis spectroscopy, dynamic light scattering (DLS), small-angle neutron scattering (SANS), and molecular dynamics (MD) simulations. The results suggest that despite being visibly absent of large aggregates in solution, the **LP** has a

strong thermodynamic tendency to aggregate due to its rigid planar backbone and minimum dissolving entropy change. The small entropy change of the process also leads to remarkable robustness of the resulting aggregate at elevated temperatures. Molecular dynamics simulations on the aggregation process of these two polymers further corroborated the drastically different aggregation entropy values caused by the ladder constituent. This work provides direct physical insights into the role of chain rigidity on solution assembly and aggregation, which is important for solution processing and applications of conjugated polymers.

Experimental section

Materials

The conjugated ladder polymer **LP** and control non-ladder conjugated polymer **CP** were synthesized based on the method reported previously.¹⁶ The chemical structures of the investigated polymers are listed in Fig. 1(a). The **LP** was synthesized in two steps, including (i) a step-growth polymerization of two alkene-functionalized monomers to give a polymeric intermediate with preorganized pendant alkene groups and (ii) subsequently a ring-closing olefin metathesis reaction to form the second thread of the σ - σ bond along the polymer backbone. The molar mass and dispersity (D) were obtained using a TOSOH EcoSEC (HLC-8320GPC) system at 40 °C with a UV detector at 254 nm and THF as the eluent. The molar masses were calculated using a calibration curve based on the UV absorption signal of polystyrene standards. The solvents chloroform, chlorobenzene and *o*-dichlorobenzene were used as purchased (Sigma Aldrich) without further purification.

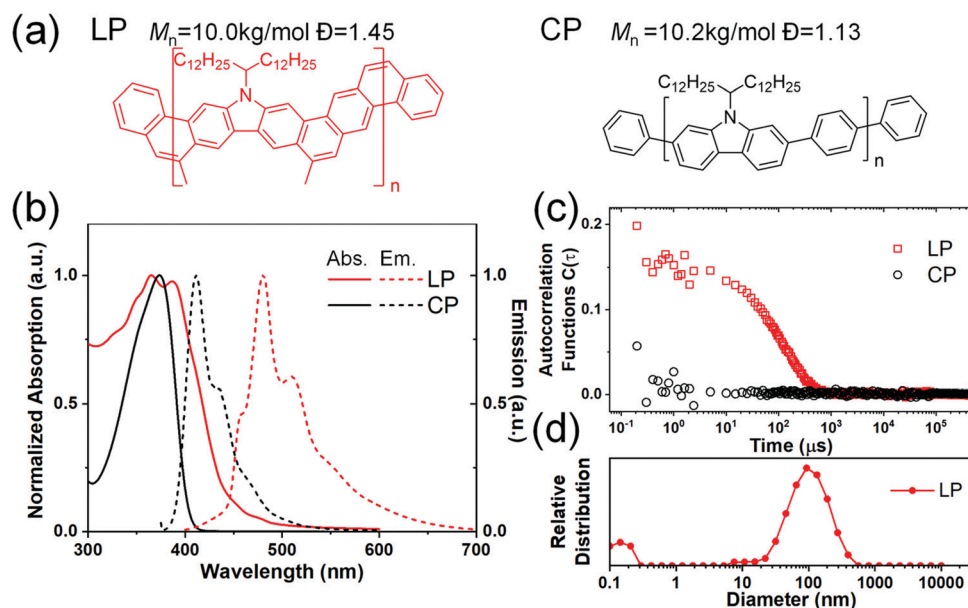


Fig. 1 (a) Structural formulas of the **LP** and **CP** used in this work. The molecular weight and distribution are labeled. (b) Normalized UV-vis absorption (solid lines) and photoluminescence spectra (dashed lines) of the **LP** and **CP** in chloroform ($\sim 0.05 \text{ mg ml}^{-1}$) at 20 °C. (c) Autocorrelation functions of the **LP** and **CP** in the chloroform solvent. (d) Size distribution of **LP** aggregates by the intensity in the solution as a function of the particle diameter.

Methods

UV-vis spectroscopy. UV-vis spectroscopy was performed using a Cary 5000 UV-Vis-NIR spectrophotometer (Agilent Technologies) with a 10 mm optical path quartz cuvette and customized-built heating elements. A solution is filtered through a 0.45 μm PTFE filter (GE healthcare) and heated to the desired temperature before the spectrum is recorded.

Photoluminescence spectroscopy. Photoluminescence spectroscopy was performed using a PTI-Horiba QuantaMaster 400 Spectrofluorimeter equipped with a 75 W Xe arc lamp in steady-state mode. The solution after filtration was placed in a 10 mm quartz cuvette at 25 ± 0.5 °C for the measurement.

Dynamic light scattering (DLS). Dynamic light scattering was performed using a Brookhaven BI-200SM research goniometer with a BI-APD avalanche photodiode detector and a 35 mW 633 nm laser source with a right-angle geometry. Solutions were kept in a capped glass tube and the temperature was controlled using an intracooler with cyclic water with a variation of 1 °C. An autocorrelation function, $C(t)$, is calculated based on the fluctuation signal:

$$C(t) = Ae^{-2\Gamma t} + B$$

where A is the optical constant through the instrument design, Γ is the relaxation of the fluctuation, t is the time and B is the constant background. Γ and q are defined as $\Gamma = Dq^2$ and the scattering vector $q = \frac{4\pi n_0}{\lambda_0} \sin\left(\frac{\theta}{2}\right)$. The size distribution of the particles was analyzed using the Brookhaven software by cumulants analysis.

Small-angle neutron scattering (SANS). SANS experiments were performed using an extended Q -range small-angle neutron scattering diffractometer (EQ-SANS BL-6) with the Spallation Neutron Source (SNS) located at Oak Ridge National Laboratory (ORNL).³² Polymers were dissolved in deuterated chlorobenzene at a concentration of 5 mg ml⁻¹ without further filtration. The solution was placed in Hellma quartz cells with a beam path of 2 mm. To cover the range of scattering wave vector q from 0.003 to 0.7 Å⁻¹, two configurations (4 m sample-to-detector distance with a wavelength band of $\lambda_{\text{min}} = 12$ Å and 2.5 m sample-to-detector distance with $\lambda_{\text{min}} = 2.5$ Å) were used. The experiments were performed at 75 °C. The scattering intensity was reduced by subtracting the background from solvents and cells and placed on an absolute scale (cm⁻¹) using a standard porous silica sample.³³ The scattering signal was analyzed using the SasView software and fitted with suitable models as described later.

Atomic force microscopy (AFM). The thin film was spin coated onto a clean silicon wafer from the chloroform solution. The AFM images of the spin coated LP and CP films were acquired using an Asylum Research Cypher S instrument operating in a tapping mode in air.

Grazing-incidence wide-angle X-ray scattering (GI-WAXS). The GIWAXS of polymeric thin films on the silicon substrate was performed using a laboratory beamline system (Xenocs Inc. Xeuss 2.0) with an X-ray wavelength of 1.54 Å and a

sample-to-detector distance of 15 cm. An incidence angle of 0.2° was used. Samples were placed under vacuum to minimize air scattering. Diffraction images were recorded using a Pilatus 1 M detector (Dectris Inc.) with an exposure time of 1.5 h and processed using the Nika software package, in combination with WAXSTools using Wavemetrics Igor.

Molecular dynamics simulations. The simulation of the aggregation of the CP and LP is challenging due to the number of potential degrees of freedom in the system and the importance of solvent effects. Two types of simulations were implemented in tandem to efficiently explore the conformational landscape without sacrificing the robust treatment of the aggregation thermodynamics. The chains were simulated first using Brownian dynamics (BD) simulation with an implicit solvent. Here, the frictional and random forces are added to a conventional molecular dynamics of the polymer, allowing for an accounting of the dynamic effects of the solvent at a lower computational cost. This allows for the initial simulations to access much longer simulated timescales than could be accessed by atomistic solvent simulations.

The simulation workflow is shown in Fig. S1 (ESI[†]). First, a single polymer chain of the CP (with 16 repeat units) or LP (8 repeat units) was placed in the center of a cubic box (side length 20 nm) with an implicit solvent and equilibrated for 5 ns using Brownian dynamics. Then, 10 of the equilibrated polymer chains were inserted into new 20 × 20 × 20 nm cubic boxes to make the concentrated CP or LP systems. Each system was further equilibrated with the implicit solvent under the same condition for another 10 ns. The initial and final configurations of these implicit solvent simulations were then explicitly solvated using a pre-equilibrated 1,2-dichlorobenzene solvent. Then, all-atomic MD simulations were carried out to each of these systems using a leap-frog integrator with a 2 fs time step. The entropies of the systems were calculated using the two-phase thermodynamics (2PT) model^{34,35} using the DoSPT code developed by Caro and co-workers.^{36,37} All simulations were carried out at 384 K and repeated eight times for statistics. Further details of the simulation process can be found in the ESI[†].

Results and discussion

The carbazole-derived polymer LP (Fig. 1(a)) is selected as a representative model for the cLP because (i) it has a very low level of defects along the ladder-type backbone on account of the highly efficient thermodynamic annulation method (ring-closing olefin metathesis) for its synthesis¹⁶ and (ii) it possesses good apparent dispersibility in solution despite the ladder-type constitution. We aim to compare the solution assembly of the LP with its non-ladder polymer counterpart CP (Fig. 1(a)). Both the LP and CP were synthesized in fresh batches with a similar molecular weight in this study. They both can be dissolved/dispersed in common organic solvents and give apparently clear solutions. The solutions of the LP and CP can pass through 0.45 μm filter membranes and give clear UV/vis absorption and fluorescent emission spectra (Fig. 1(b)). Our previous study³⁸ on

the optical properties of the **LP** suggested the formation of a H-aggregate in solution. The lowest energy absorption band of the **LP** (~ 450 nm)^{16,38} is extremely weak and can be easily ignored. Considering this absorption peak and the lowest energy emission peak at 456 nm (Fig. S2, ESI[†]), the **LP** exhibits an extremely small Stokes shift as expected for a highly rigid conjugated ladder polymer. Here, dynamic light scattering (DLS) was performed to probe the solution aggregation of the **LP** and **CP** (Fig. 1(c)). It is noteworthy that neither the **LP** nor the **CP** absorbs the wavelength of laser used in the DLS study (633 nm) so that no absorptive interference is encountered during the measurement. The aggregation formation of the **LP** was confirmed by DLS, which showed a single decay in the autocorrelation function, corresponding to aggregation with an average hydrodynamic radius of 100 nm. The **CP** solution, in contrast, gave a flat signal, indicating that the **CP** is fully dissolved in chloroform.

To test the potential dissociation of these aggregates under variable conditions, we performed UV-vis spectroscopy for the **LP** dispersed in several different solvents at varied temperatures. 1-Chloronaphelene (CN) and chlorobenzene (CB) were selected as the solvents because they are known to be highly efficient in breaking pi-pi aggregates and can be heated to high temperatures thanks to their high boiling points.³⁹ As shown in Fig. 2(a) and (b), when dispersed in these solvents, the **LP** showed similar absorption profiles to that in chloroform. Remarkably, at higher temperatures (up to 200 °C for CN and 120 °C for CB), the solution spectra of the **LP** remained almost the same with only a marginal change of the ratio of 0–0/0–1 peaks, despite the fact that the **LP** aggregated in solution. In contrast, for the **CP** solution in CB, the absorption peaks showed a red shift from 378 nm at 20 °C to 375 nm at 120 °C (Fig. S3, ESI[†]) due to the conformational change of the fully dissolved chains. The variable UV-vis spectra of the **LP** were also recorded in other solvents such as chloroform and dichlorobenzene, all showing similar peak profiles to marginal changes upon heating as shown in Fig. S4 (ESI[†]). This observation indicates that **LP** chains maintained their aggregation form, and there is no significant conformational change on the ladder-type backbone at elevated temperatures as high as 200 °C. Notably, this weak temperature dependence of absorption is also observed independently in other conjugated ladder polymers.³¹ This behavior is typically not observed on conventional, non-ladder type conjugated polymers.^{40–42} The stable aggregation of the **LP** at high temperatures was also confirmed by DLS as the hydrodynamic radius remained constant at elevated temperatures up to the limit of our instrument (75 °C) (Fig. 2(c)). Variable concentration DLS measurements were also carried out on the **LP** (Fig. 2(d)), as it is known that decreasing the concentration can break the **LP** aggregation.³⁸ These DLS data show that the **LP** remained aggregated at concentrations as low as 0.05 mg ml⁻¹ in the CB solution and 0.005 mg ml⁻¹ in the chloroform solution (Fig. S5, ESI[†]). We also tested the DLS of a low molecular weight batch of the oligomeric **LP** ($M_n \sim 3$ kg mol⁻¹), showing a peak hydrodynamic radius of 30 nm (Fig. S6, ESI[†]), suggesting significant

aggregation even for this low molecular weight batch. Our finding indicates that the aggregation of the **LP** in various solutions is highly robust and insensitive to solution temperatures.

To further characterize the aggregation of the **LP**, we conducted small-angle neutron scattering (SANS) on both the **LP** and **CP** solutions dissolved in deuterated chlorobenzene at 75 °C. As shown in Fig. 3(c), the scattering profile of the **LP** never reaches its Guinier region in the measurement range ($0.008 \text{ \AA}^{-1} < Q < 0.3 \text{ \AA}^{-1}$), as indicated by the scattering intensity continuing to increase at the low q region, following the trend of $I \propto q^{-1.76}$. These data suggested that the **LP** solution forms large aggregate under the experimental conditions. In contrast, the scattering profile of the **CP** reached the Guinier region as evidenced from a plateau at lower q , suggesting well-dispersed polymer chains in solution. Hence, we used two different fitting models to fit the curves, namely the parallelepiped model⁴³ for the **LP** and the flexible cylinder model⁴⁴ for the **CP**. The fitting parameters are shown in Fig. 3. The **LP** can be modeled by elongated parallelepiped model with a large dimension of $c = 1978.8 \text{ \AA}$, which was much larger than a single-chain contour length (around 17.9 nm, see Fig. S7, ESI[†]) so it must be an aggregated package of multiple chains. The **CP** has a contour length (L_c) of 122.7 Å and a small cylinder diameter (R) of 8.9 Å, which is reasonable for a dissolved non-ladder single chain with a molar mass of around 10 kg mol⁻¹. Temperature-dependent SANS on the **LP** also showed the presence of large aggregates at 25 °C and 50 °C (Fig. S8 and Table S1, ESI[†]), which was in accordance with the UV-vis and DLS results. These data demonstrate the size and robustness of **LP** aggregates in solution. It is also noteworthy that the single-chain conformation of the **LP** cannot be directly probed by SANS due to its strong aggregation in the wide temperature range we have measured.

To elucidate the chain packing mode in the **LP** aggregates, we conducted atomic force microscopy (AFM) and grazing incidence wide-angle X-ray scattering (GI-WAXS) on the **LP** thin film. Because the **LP** aggregates are stable towards heat and solvents, the morphology to chain aggregate is expected to be maintained from the solution to the solid-state through a spin coating process. On the samples spun coated from a dilute solution (Fig. S9, ESI[†]), we only observed round particles on the wafer rather than large thin sheets seen on other conjugated polymers assembled by strong π - π stacking.^{45,46} The thicker **LP** film (40 nm) was prepared by drop-casting chloroform solution onto the silicon wafer, and the GI-WAXS result only showed a broad isotropic scattering peak without a strong scattering profile (Fig. S10, ESI[†]), indicating an amorphous nature of the **LP** aggregates. This observation does not contradict the rigid chain feature, as a similar behavior has been observed in many rigid rod polymers.⁴⁷ This amorphous feature was also reported in other fully conjugated ladder polymers,^{16,48} although thermal annealing on solid films can improve the crystallinity of certain ladder polymers⁴⁹ and rigid conjugated polymers.^{50,51} The absence of crystallinity in fully conjugated ladder polymers can be attributed to the (i) strong dynamic aggregation already formed in solution and (ii) the lack of the

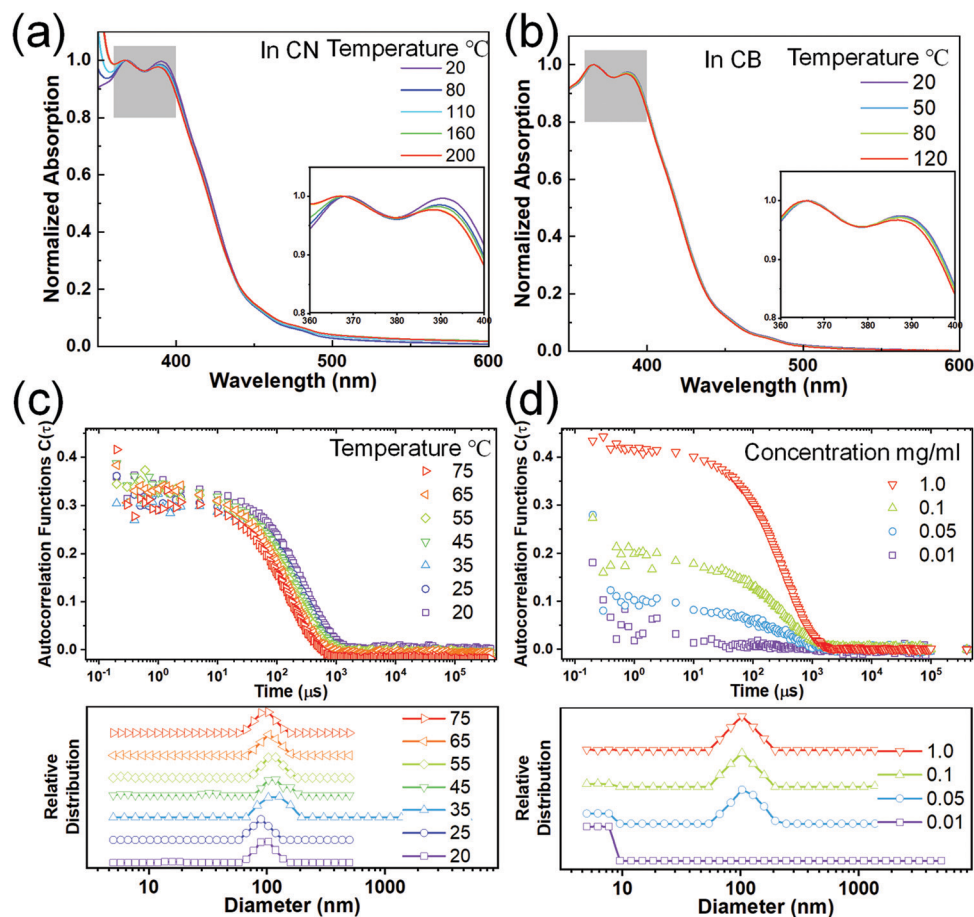


Fig. 2 Variable temperature UV-vis spectra of the LP in (a) chloronaphthalene (CN) and (b) chlorobenzene (CB) normalized by 0–1 peaks. The inset shows a magnified view of the gray area. Temperature-dependent (c) and concentration-dependent (d) DLS results of the LP in chlorobenzene and the corresponding size distribution.

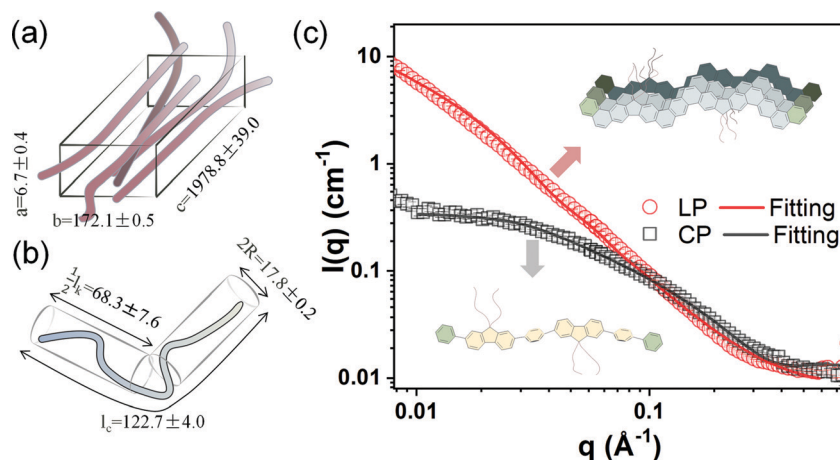


Fig. 3 Chain model and fitting results for SANS analysis (length unit in Å): (a) Parallelepiped model for the LP and (b) flexible cylinder model for the CP. (c) SANS data and fitting curve. The inset illustrates the chain conformation of the LP (top) and CP (bottom).

chain mobility of the large and rigid polymer backbone during the transition from solution to the solid state, as demonstrated in our previous systematic study on a series of ladder-type oligomers.⁵² This lack of crystalline domain and the presence

of the long alkyl side-chain prevents fast charge transport in the solid state of the LP as mentioned previously.¹⁶

We hypothesized that the lack of the temperature dependence of LP aggregation was a result of small entropy changes

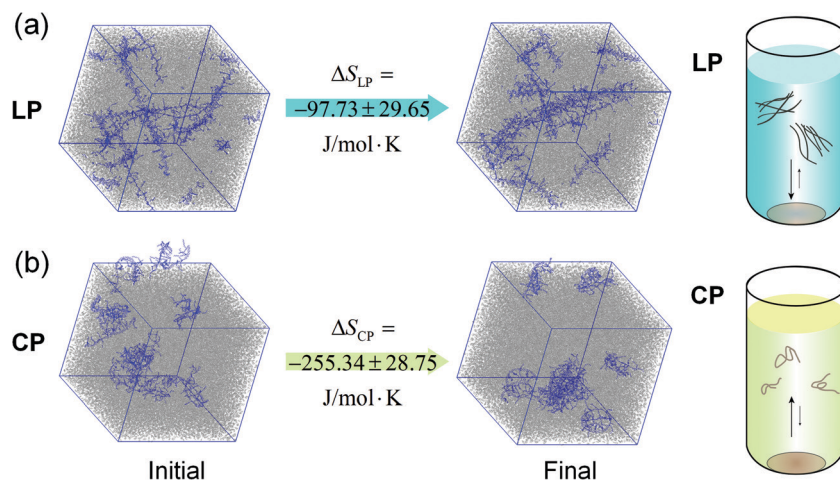


Fig. 4 Snapshots of the initial and final chain conformations of the **LP** (a) and **CP** (b) from a single simulation. The polymer chains are colored in blue and the atomic solvents are colored in gray. The entropy changes associated with the aggregation processes were shown above. An illustration of the dissolving process of the **LP** and **CP** is shown next to it.

during the process. It is envisioned and demonstrated that a ladder type polymer chain possesses a much lower initial entropy compared to conventional polymers with free torsional motions about the main chain. Thereby, the aggregation of such rigid ladder-type chains would induce minimal restriction on the degree of freedom of the chain and hence impose a much smaller entropy cost for aggregation. To test this hypothesis, the molecular simulations were performed to elucidate the entropy change during the aggregation process in *o*-dichlorobenzene. The results of one of the eight simulations are shown in Fig. 4, illustrating the chain conformation before and after energy optimization. As expected, the **LP** is straighter after the energy optimization, but it contains a select number of twists and bends that require much longer time to be flattened, in agreement with reports on another ladder polymer.⁵³ The entropy change of this process is calculated using the formula:

$$\Delta S_{\text{LP}} = S_{\text{dissolved LP}} - S_{\text{solid LP}} \text{ and } \Delta S_{\text{CP}} = S_{\text{dissolved CP}} - S_{\text{solid CP}},$$

where $S_{\text{dissolved}}$ and S_{solid} are the total entropy of the polymer system at initial and final states, respectively. The difference of these states represents the reverse of the dissolving process. The calculated entropy values from eight individual simulations are listed in Table S2 (ESI[†]) and the cluster analysis to monitor the aggregation process from the BD simulations is shown in Fig. S11 (ESI[†]). At the end of the simulation procedures, the **LP** has fewer aggregated clusters and larger cluster sizes compared to the **CP**. Although both ΔS_{LP} and ΔS_{CP} are negative for these processes, indicating that the entropy lost during aggregation, the ΔS_{LP} value ($-97.73 \pm 29.65 \text{ J mol}^{-1} \text{ K}^{-1}$) was significantly smaller in the absolute value compared with the ΔS_{CP} value ($-255.34 \pm 28.75 \text{ J mol}^{-1} \text{ K}^{-1}$), representing a significantly less entropy cost for the **LP** to aggregate, and hence a much smaller temperature-dependent process for its dissolution and aggregation. These computational results also indicate that the much bulky side chain is necessary to fully dissolve rigid ladder polymers by compensating the low entropy gain during dissolution.²²

We expect that the low temperature dependence of aggregation can be ubiquitous among other rigid ladder polymers. This feature should be considered and perhaps exploited as a critical feature during the solution processing of ladder polymers for solid state applications. For example, if a polymer aggregation feature in solution needs to be maintained in the solid state through solution processing and thermal annealing, a rigid ladder-type backbone can be designed to give the desired robustness for the aggregation, which is insensitive to thermal annealing and solvent attack.

Conclusions

To conclude, we characterized the solution aggregation properties of a low-defect conjugated ladder polymer **LP** and its non-ladder conjugated polymer control **CP** by temperature-dependent UV-vis spectroscopy, DLS, and small-angle neutron scattering investigations, combined with molecular dynamics simulation. We elucidated that the **LP** forms stable aggregates in solution and remains aggregated at elevated temperatures up to 200 °C. We also demonstrated the amorphous nature of the aggregation in solution and in the thin film state for the GI-WAXS measurement. The Brownian dynamics simulation showed that the **LP** had a low entropy decrease during the chain aggregation process caused by the low-entropy rigid ladder-type backbone. These results highlight the role of the chain conformation in the thermodynamic properties of rigid ladder polymers in solution and in the solid state. The small temperature dependence of ladder polymer aggregation should be considered and exploited during the solution processing of these materials for solid state applications.

Author contributions

Guorong Ma performed the characterization of the **LP** and **CP** using UV-Vis/PL/DLS/AFM/GI-WAXS. Mingwan Leng and Yirui Cao synthesized and purified the **LP** and **CP** and characterized

by NMR/GPC. Zhiqiang Cao performed the SANS experiments and analyzed the data. Shi Li and Daniel P. Tabor designed, conducted, and analyzed the MD simulations. The manuscript was written by Guorong Ma and Mingwan Leng. All the authors gave approval to the final version of the manuscript. Xiaodan Gu and Lei Fang conceived the idea, coordinated, and supervised the research project.

Conflicts of interest

The authors declare no competing financial interest.

Acknowledgements

This work was financially supported by the U.S. National Science Foundation (NSF) under award number of No. CHE 2004133 and 2003733. We thank the Center for Nanophase Materials Sciences under the support of DOE for the SANS characterization. This work benefited from the use of the SasView application, originally developed under the NSF Award DMR-0520547. SasView contains the code developed with funding from the European Union's horizon 2020 research and innovation programme under the SINE20. D. P. T. and S. L. acknowledge support from the Texas A&M University Startup Funding. Portions of this research were conducted with high-performance research computing resources provided by Texas A&M University HPRC. D. P. T. acknowledges the Texas A&M Institute of Data Science Career Initiation Fellowship.

Notes and references

- H. Sirringhaus, 25th anniversary article: Organic field-effect transistors: The path beyond amorphous silicon, *Adv. Mater.*, 2014, **26**(9), 1319–1335.
- Z. Bao and X. Chen, Flexible and stretchable devices, *Adv. Mater.*, 2016, **28**(22), 4177–4179.
- J. Onorato, V. Pakhnyuk and C. K. Luscombe, Structure and design of polymers for durable, stretchable organic electronics, *Polym. J.*, 2016, **49**(1), 41–60.
- X. Gu, Y. Zhou, K. Gu, T. Kurosawa, Y. Guo, Y. Li, H. Lin, B. C. Schroeder, H. Yan, F. Molina-Lopez, C. J. Tassone, C. Wang, S. C.-B. Mannsfeld, H. Yan, D. Zhao, M. F. Toney and Z. Bao, Roll-to-roll printed large-area all-polymer solar cells with 5% efficiency based on a low crystallinity conjugated polymer blend, *Adv. Energy Mater.*, 2017, **7**(14), 1602742.
- J. Xu, H. C. Wu, C. Zhu, A. Ehrlich, L. Shaw, M. Nikolka, S. Wang, F. Molina-Lopez, X. Gu, S. Luo, D. Zhou, Y. H. Kim, G. N. Wang, K. Gu, V. R. Feig, S. Chen, Y. Kim, T. Katsumata, Y. Q. Zheng, H. Yan, J. W. Chung, J. Lopez, B. Murmann and Z. Bao, Multi-scale ordering in highly stretchable polymer semiconducting films, *Nat. Mater.*, 2019, **18**(6), 594–601.
- J. Wang, C. Zhao, L. Zhou, X. Liang, Y. Li, G. Sheng, Z. Du and J. Tang, An effective strategy to design a large bandgap conjugated polymer by tuning the molecular backbone curvature, *Macromol. Rapid Commun.*, 2021, **42**(10), 2000757.
- J. Lee, A. J. Kalin, T. Yuan, M. Al-Hashimi and L. Fang, Fully conjugated ladder polymers, *Chem. Sci.*, 2017, **8**(4), 2503–2521.
- P. Prins, F. C. Grozema, J. M. Schins, S. Patil, U. Scherf and L. D. Siebbeles, High intrachain hole mobility on molecular wires of ladder-type poly(*p*-phenylenes), *Phys. Rev. Lett.*, 2006, **96**(14), 146601.
- M. Kertesz and T. R. Hughbanks, Low bandgap ladder polymers, *Synth. Met.*, 1995, **69**(1-3), 699–700.
- A. Tsuda and A. Osuka, Fully conjugated porphyrin tapes with electronic absorption bands that reach into infrared, *Science*, 2001, **293**(5527), 79–82.
- S. Wang, W. Hong, S. Ren, J. Li, M. Wang, X. Gao and H. Li, New ladder-type conjugated polymer with broad absorption, high thermal stability, and low band gap, *J. Polym. Sci., Part A: Polym. Chem.*, 2012, **50**(20), 4272–4276.
- Y. Zou, X. Ji, J. Cai, T. Yuan, D. J. Stanton, Y.-H. Lin, M. Naraghi and L. Fang, Synthesis and solution processing of a hydrogen-bonded ladder polymer, *Chem*, 2017, **2**(1), 139–152.
- U. Scherf and K. Müllen, A soluble ladder polymer via bridging of functionalized poly(*p*-phenylene)-precursors, *Rapid Commun.*, 1991, **12**(8), 489–497.
- S. A. Jenekhe and P. O. Johnson, Complexation-mediated solubilization and processing of rigid-chain and ladder polymers in aprotic organic solvents, *Macromolecules*, 1990, **23**(20), 4419–4429.
- C. Huang, S. Barlow and S. R. Marder, Perylene-3,4,9,10-tetracarboxylic acid diimides: Synthesis, physical properties, and use in organic electronics, *J. Org. Chem.*, 2011, **76**(8), 2386–2407.
- J. Lee, B. B. Rajeeva, T. Yuan, Z. H. Guo, Y. H. Lin, M. Al-Hashimi, Y. Zheng and L. Fang, Thermodynamic synthesis of solution processable ladder polymers, *Chem. Sci.*, 2016, **7**(2), 881–889.
- F. Trilling, M.-K. Ausländer and U. Scherf, Ladder-type polymers and ladder-type polyelectrolytes with on-chain dibenz[*a,h*]anthracene chromophores, *Macromolecules*, 2019, **52**(8), 3115–3122.
- M. Grandl, J. Schepper, S. Maity, A. Peukert, E. von Hauff and F. Pammer, N → B Ladder polymers prepared by postfunctionalization: Tuning of electron affinity and evaluation as acceptors in all-polymer solar cells, *Macromolecules*, 2019, **52**(3), 1013–1024.
- Y. Cao, C. Zhu, M. Barlog, K. P. Barker, X. Ji, A. J. Kalin, M. Al-Hashimi and L. Fang, Electron-deficient polycyclic pi-system fused with multiple B ← N coordinate bonds, *J. Org. Chem.*, 2021, **86**(3), 2100–2106.
- Q. Wang, J. Qi, W. Qiao and Z. Y. Wang, Soluble ladder conjugated polypyrrones: Synthesis, characterization and application in photodetectors, *Dyes Pigm.*, 2015, **113**, 160–164.
- S. Qiu, P. Lu, X. Liu, F. Shen, L. Liu, Y. Ma and J. Shen, New ladder-type poly(*p*-phenylene)s containing fluorene unit exhibiting high efficient electroluminescence, *Macromolecules*, 2003, **36**(26), 9823–9829.
- F. S. Kim, C. H. Park, Y. Na and S. A. Jenekhe, Effects of ladder structure on the electronic properties and field-effect

- transistor performance of Poly(benzobisimidazobenzophenanthroline), *Org. Electron.*, 2019, **69**, 301–307.
- 23 S. Wang, H. Sun, U. Ail, M. Vagin, P. O. Persson, J. W. Andreasen, W. Thiel, M. Berggren, X. Crispin, D. Fazzi and S. Fabiano, Thermoelectric properties of solution-processed n-doped ladder-type conducting polymers, *Adv. Mater.*, 2016, **28**(48), 10764–10771.
- 24 Y. X. Xu, C. C. Chueh, H. L. Yip, F. Z. Ding, Y. X. Li, C. Z. Li, X. Li, W. C. Chen and A. K. Jen, Improved charge transport and absorption coefficient in indacenodithieno[3,2-*b*]thiophene-based ladder-type polymer leading to highly efficient polymer solar cells, *Adv. Mater.*, 2012, **24**(47), 6356–6361.
- 25 P. Sakthivel, H. S. Song, N. Chakravarthi, J. W. Lee, Y.-S. Gal, S. Hwang and S.-H. Jin, Synthesis and characterization of new indeno[1,2-*b*]indole-*co*-benzothiadiazole-based π -conjugated ladder type polymers for bulk heterojunction polymer solar cells, *Polymer*, 2013, **54**(18), 4883–4893.
- 26 Y. L. Chen, W. S. Kao, C. E. Tsai, Y. Y. Lai, Y. J. Cheng and C. S. Hsu, A new ladder-type benzodi(cyclopentadithiophene)-based donor-acceptor polymer and a modified hole-collecting PEDOT:PSS layer to achieve tandem solar cells with an open-circuit voltage of 1.62 V, *Chem. Commun.*, 2013, **49**(70), 7702–7704.
- 27 M. Lee, S.-J. Hahn, T.-H. Kim and A. Phenylene-alkylated, Thiophene-based partially ladder-type conjugated polymer, *Bull. Korean Chem. Soc.*, 2013, **34**(8), 2495–2498.
- 28 X. Shao, C. Dou, J. Liu and L. Wang, A new building block with intramolecular D–A character for conjugated polymers: Ladder structure based on B ← N unit, *Sci. China: Chem.*, 2019, **62**(10), 1387–1392.
- 29 G. Petekidis, G. Fytas, U. Scherf, K. Mllen and G. Fleischer, Dynamics of poly(*p*-phenylene) ladder polymers in solution, *J. Polym. Sci., Part B: Polym. Phys.*, 1999, **37**(16), 2211–2220.
- 30 S. Che, J. Pang, A. J. Kalin, C. Wang, X. Ji, J. Lee, D. Cole, J.-L. Li, X. Tu, Q. Zhang, H.-C. Zhou and L. Fang, Rigid ladder-type porous polymer networks for entropically favorable gas adsorption, *ACS Mater. Lett.*, 2019, **2**(1), 49–54.
- 31 Y.-W. Huang, Y.-C. Lin, J.-S. Li, W.-C. Chen and C.-C. Chueh, Investigating the backbone conformation and configuration effects for donor–acceptor conjugated polymers with ladder-type structures synthesized through Aldol polycondensation, *J. Mater. Chem. C*, 2021, **9**(30), 9473–9483.
- 32 J. K. Zhao, C. Y. Gao and D. Liu, The extended Q-range small-angle neutron scattering diffractometer at the SNS, *J. Appl. Crystallogr.*, 2010, **43**(5), 1068–1077.
- 33 W. T. Heller, M. Cuneo, L. Debeer-Schmitt, C. Do, L. He, L. Heroux, K. Littrell, S. V. Pingali, S. Qian and C. Stanley, The suite of small-angle neutron scattering instruments at Oak ridge national laboratory, *J. Appl. Crystallogr.*, 2018, **51**(2), 242–248.
- 34 S.-T. Lin, M. Blanco and W. A. Goddard, The two-phase model for calculating thermodynamic properties of liquids from molecular dynamics: Validation for the phase diagram of Lennard–Jones fluids. The, *J. Chem. Phys.*, 2003, **119**(22), 11792–11805.
- 35 S. T. Lin, P. K. Maiti and W. A. Goddard 3rd, Two-phase thermodynamic model for efficient and accurate absolute entropy of water from molecular dynamics simulations, *J. Phys. Chem. B*, 2010, **114**(24), 8191–8198.
- 36 M. A. Caro, T. Laurila and O. Lopez-Acevedo, Accurate schemes for calculation of thermodynamic properties of liquid mixtures from molecular dynamics simulations, *J. Chem. Phys.*, 2016, **145**(24), 244504.
- 37 M. A. Caro, O. Lopez-Acevedo and T. Laurila, Redox potentials from *ab initio* molecular dynamics and explicit entropy calculations: Application to transition metals in aqueous solution, *J. Chem. Theory Comput.*, 2017, **13**(8), 3432–3441.
- 38 W. R. Hollingsworth, J. Lee, L. Fang and A. L. Ayzner, Exciton relaxation in highly rigid conjugated polymers: Correlating radiative dynamics with structural heterogeneity and wavefunction delocalization, *ACS Energy Lett.*, 2017, **2**(9), 2096–2102.
- 39 K. F. Zhao, Q. Zhang, L. Chen, T. Zhang and Y. C. Han, Nucleation and growth of P(NDI2OD-T2) nanowires *via* side chain ordering and backbone planarization, *Macromolecules*, 2021, **54**(5), 2143–2154.
- 40 W. Ma, G. Yang, K. Jiang, J. H. Carpenter, Y. Wu, X. Meng, T. McAfee, J. Zhao, C. Zhu, C. Wang, H. Ade and H. Yan, Influence of processing parameters and molecular weight on the morphology and properties of high-performance PffBT4T-2OD:PC71BM organic solar cells, *Adv. Energy Mater.*, 2015, **5**(23), 1501400.
- 41 G. H.-L. Heintges, P. J. Leenaers and R. A.-J. Janssen, The effect of side-chain substitution and hot processing on diketopyrrolopyrrole-based polymers for organic solar cells, *J. Mater. Chem. A*, 2017, **5**(26), 13748–13756.
- 42 R. Heuvel, F. J.-M. Colberts, J. Li, M. M. Wienk and R. A.-J. Janssen, The effect of side-chain substitution on the aggregation and photovoltaic performance of diketopyrrolopyrrole-*alt*-dicarboxylic ester bithiophene polymers, *J. Mater. Chem. A*, 2018, **6**(42), 20904–20915.
- 43 J. K. Keum, K. Xiao, I. N. Ivanov, K. Hong, J. F. Browning, G. S. Smith, M. Shao, K. C. Littrell, A. J. Rondinone, E. Andrew Payzant, J. Chen and D. K. Hensley, Solvent quality-induced nucleation and growth of parallelepiped nanorods in dilute poly(3-hexylthiophene) (P3HT) solution and the impact on the crystalline morphology of solution-cast thin film, *CrystEngComm*, 2013, **15**(6), 1114–1124.
- 44 J. S. Pedersen and P. Schurtenberger, Scattering Functions of Semiflexible Polymers with and without Excluded Volume Effects, *Macromolecules*, 1996, **29**(23), 7602–7612.
- 45 J. Zhu, Y. Han, R. Kumar, Y. He, K. Hong, P. V. Bonnesen, B. G. Sumpter, S. C. Smith, G. S. Smith, I. N. Ivanov and C. Do, Controlling molecular ordering in solution-state conjugated polymers, *Nanoscale*, 2015, **7**(37), 15134–15141.
- 46 Z. F. Yao, Z. Y. Wang, H. T. Wu, Y. Lu, Q. Y. Li, L. Zou, J. Y. Wang and J. Pei, Ordered solid-state microstructures of conjugated polymers arising from solution-state aggregation, *Angew. Chem., Int. Ed.*, 2020, **59**(40), 17467–17471.
- 47 R. A. Gaudiana, R. A. Minns, R. Sinta, N. Weeks and H. G. Rogers, Amorphous rigid-rod polymers, *Prog. Polym. Sci.*, 1989, **14**(1), 47–89.
- 48 S. R. Bheemireddy, M. P. Hautzinger, T. Li, B. Lee and K. N. Plunkett, Conjugated ladder polymers by a cyclopentannulation polymerization, *J. Am. Chem. Soc.*, 2017, **139**(16), 5801–5807.

